



## Highly conductive and transparent coatings from flow-aligned silver nanowires with large electrical and optical anisotropy

Ye Xu, Dengteng Ge, Gabriel A Calderon-Ortiz, Annemarie L Exarhos, Coline Bretz, Ahmed M. Alsayed, Dave Kurz, J M Kikkawa, Rémi Dreyfus, Shu Yang, et al.

### ► To cite this version:

Ye Xu, Dengteng Ge, Gabriel A Calderon-Ortiz, Annemarie L Exarhos, Coline Bretz, et al.. Highly conductive and transparent coatings from flow-aligned silver nanowires with large electrical and optical anisotropy. *Nanoscale*, Royal Society of Chemistry, 2020, 12 (11), pp.6438-6448. 10.1039/c9nr09598e . hal-02567539

**HAL Id: hal-02567539**

**<https://hal.archives-ouvertes.fr/hal-02567539>**

Submitted on 15 May 2020

**HAL** is a multi-disciplinary open access archive for the deposit and dissemination of scientific research documents, whether they are published or not. The documents may come from teaching and research institutions in France or abroad, or from public or private research centers.

L'archive ouverte pluridisciplinaire **HAL**, est destinée au dépôt et à la diffusion de documents scientifiques de niveau recherche, publiés ou non, émanant des établissements d'enseignement et de recherche français ou étrangers, des laboratoires publics ou privés.

# 1 Highly Conductive and Transparent Coatings from Flow-aligned 2 Silver Nanowires with Large Electric and Optical Anisotropy<sup>†</sup>

3 Ye Xu,<sup>‡\*abc</sup> Dengteng Ge,<sup>‡de</sup> Gabriel A. Calderon-Ortiz,<sup>b</sup> Annemarie L. Exarhos,<sup>b§</sup> Coline Bretz,<sup>c</sup>  
4 Ahmed Alsayed,<sup>c</sup> Dave Kurz,<sup>b</sup> J. M. Kikkawa,<sup>b</sup> Remi Dreyfus,<sup>c</sup> Shu Yang,<sup>d</sup> and A. G. Yodh<sup>b</sup>

5

6 <sup>a</sup>*School of Mechanical Engineering and Automation and Center of Soft Matter Physics and its*  
7 *Applications, Beihang University, Beijing 100191, P.R. China. Email: [ye.xu@buaa.edu.cn](mailto:ye.xu@buaa.edu.cn)*

8 <sup>b</sup>*Department of Physics and Astronomy, University of Pennsylvania, Philadelphia, Pennsylvania*  
9 *19104, USA*

10 <sup>c</sup>*Complex Assemblies of Soft Matter, CNRS-Solvay-UPenn UMI 3254, Bristol, Pennsylvania 19007, USA*

11 <sup>d</sup>*Department of Materials Science and Engineering, University of Pennsylvania, Philadelphia,*  
12 *Pennsylvania 19104, USA*

13 <sup>e</sup>*State Key Laboratory for Modification of Chemical Fibers and Polymer Materials, Institute of*  
14 *Functional Materials, Donghua University, Shanghai 201620, P.R. China*

15

16 Conductive and transparent coatings consisting of silver nanowires (AgNWs) are  
17 promising candidates for emerging flexible electronics applications. Coatings of aligned  
18 AgNWs offer unusual electronic and optical anisotropies, with potential for micro-circuits,  
19 antennas, and polarization sensors. Here we explore a microfluidics setup and flow-induced  
20 alignment mechanisms to create centimeter-scale highly conductive coatings of aligned

1 AgNWs with order parameters reaching 0.84, leading to large electrical and optical  
2 anisotropy. By varying flow rates, we establish the relation between the shear rate and the  
3 alignment and investigate possible alignment mechanisms. The angle-dependent sheet  
4 resistance of the aligned AgNW networks exhibits an electronic transport anisotropy of  
5  $\sim 10\times$  while maintaining low resistivity ( $< 50 \Omega/\text{sq}$ ) in all directions. When illuminated, the  
6 aligned AgNW coatings exhibit angle- and polarization-dependent color, and the polarized  
7 reflection anisotropy can be as large as 25. This large optical anisotropy is due to a  
8 combination of alignment, polarization response, and angle-dependent scattering of the  
9 aligned AgNWs.

10

11

12 <sup>†</sup>Electronic supplementary information (ESI) available.

13 <sup>‡</sup>Authors of equal contributions.

14 <sup>§</sup>Present address: Department of Physics, Lafayette College, Easton, PA 18042, USA

# 1 Introduction

2 The large aspect ratio and electrical conductivity of silver nanowires (AgNWs) offer promising  
3 ingredients for emerging electronic and optical applications, including conducting inks and pastes  
4 used in circuits.<sup>1,2</sup> AgNW films, for example, are attractive candidates for transparent conductive  
5 coatings in flexible touch-screen displays, due to their high visible light transparency and  
6 tolerance to planar strain.<sup>3-5</sup> Moreover, the one-dimensional (1D) nature of these wires  
7 induces anisotropy in electrical conductivity and optical appearance, and some nanowire  
8 assemblies with anisotropic properties have been found to exhibit enhanced performance  
9 in nanocomputing devices,<sup>6</sup> antennas,<sup>7-9</sup> polarized-light-based sensors,<sup>10</sup> and surface  
10 enhanced Raman spectroscopy (SERS).<sup>11</sup>

11 The performance of AgNW-based devices usually depends on the density and organization  
12 of the AgNWs. When AgNWs are used in flexible electronics to replace ITO, the combination of a  
13 *low areal* density for optical transparency and a percolated network of AgNWs for conductivity  
14 is required. In the literature, this performance is generally achieved from *isotropic* percolating  
15 nanowire networks at a *low areal* density.<sup>5,12-14</sup>

16 Films with *high areal* density of AgNWs, on the other hand, offer the possibility to  
17 generate *anisotropic* optical and electrical properties that ultimately offer many more ways  
18 to modulate signals. For example, the fabrication of AgNW-based optical elements with  
19 polarization sensitivity and the synthesis of conducting devices with anisotropic conductivity  
20 require both a high degree of alignment and a large areal density. In a related vein, the creation  
21 of plasmonic waveguides, based on single<sup>15-17</sup> or multiple<sup>9,18</sup> nanowires, could rely on plasmonic  
22 interactions among nanowires<sup>19</sup>, which would benefit from aligned nanowires with high areal

1 density. To this end, films of aligned nanowires offer the possibility to tune the coupling between  
2 individual nanowires and thus introduce novel collective responses, which could be more  
3 sensitive than conventional, continuous metal films. Moreover, nanowire films hold potential to  
4 be flexible and stretchable, which could be also useful for mechano- and thermal-sensing.

5 Many methodologies for deposition and alignment of 1D nanomaterials such as  
6 nanowires or nanotubes have been explored.<sup>10,11,20-29</sup> Self-assembly at oil-water-air  
7 interfaces<sup>25</sup> and Langmuir–Blodgett methods<sup>30</sup> have been used to align AgNWs. More  
8 recently, capillary-based techniques including capillary printing,<sup>31</sup> meniscus-dragging,<sup>32</sup> H-  
9 dip,<sup>33</sup> and bar-coating<sup>34</sup> have been used to create large-scale aligned or cross-aligned AgNW  
10 coatings on flat substrates. Nevertheless, these techniques can only print AgNWs along one  
11 specific direction,<sup>32,33</sup> or require external mechanical force.<sup>31</sup> Therefore, they are not suitable  
12 for parallel printing of complex circuitry. Microfluidic channels, where the shear force and  
13 flow geometry can be well-controlled, thus, offering more flexibility for depositing AgNW  
14 coatings with pre-designed patterns. Indeed, shear flow has been used for aligning  
15 nanotubes and nanowires. Huang *et al.*, first explored this method to align nanowires within  
16 a microfluidics apparatus.<sup>35</sup> They created nanoscale network structures with a very low areal  
17 density. Later, Liu *et al.* employed shear flow in circular glass capillaries to prepare more  
18 dense and aligned AgNW coatings.<sup>11</sup> Though very efficient, because of geometric constraints,  
19 these nanowires cover only the interior of circular glass tubes. Clearly, there remains a need  
20 for new methods to assemble AgNWs into scalable and aligned structures of high areal  
21 density with adequate light transmission, to achieve electrical and optical anisotropy for  
22 applications such as polarization light sensors and plasmonic waveguides.

1 In this contribution, we employ flow-assisted assembly to generate centimeter-scale  
2 AgNW coatings at high areal density (approximately 40% areal coverage or  $10^4$   
3 nanowires/mm<sup>2</sup>), with high conductivity ( $<10 \Omega/\text{sq}$ ), and with controlled electric and optical  
4 anisotropy on planar surfaces. The robust method enables experimental control of  
5 alignment via variation of the shear rate of the AgNW suspension near the substrate surface.  
6 We systematically investigate the angular dependence of coating sheet resistance and  
7 optical properties. These properties are strongly affected by AgNW alignment. The  
8 anisotropy of electric conductivity is  $\sim 10x$  in well-aligned AgNW coatings. Moreover, by  
9 combining polarized illumination and detection of scattered light from the aligned AgNW  
10 coatings, the degree of polarized reflection anisotropy can reach up to  $\sim 25x$ . The films also  
11 have good transparency ( $\sim 70\%$ ) in the normal incidence across the visible spectrum. The  
12 performance and features of AgNW films based on our deposition technique, along with  
13 those from previous literature, are reported in Table 1. Our transparent coatings in the  
14 planar geometry have comparatively high areal density and larger electrical and optical  
15 anisotropy due to better control of AgNW orientation and concentration. These features  
16 make them attractive for components in micro-/nano-circuits and optical sensors.

17

## 18 **Results and discussions**

### 19 **Preparation of AgNW coatings**

20 Thin coatings of AgNWs are prepared by flowing nanowire suspensions through thin  
21 rectangular microfluidic channels, as shown in Fig. 1A. At the beginning of the coating  
22 preparation, we utilize a syringe pump (Harvard Instrument) to drive the flow of 2 mL of

1 nanowire suspension through the channel at a constant volumetric flow rate,  $Q$ , ranging  
2 from 0.5 to 5 mL/min. The flow of AgNW suspension creates boundary shear at a rate  
3 ranging from  $10 \text{ s}^{-1}$  to  $1000 \text{ s}^{-1}$  near the top and bottom glass walls of the channel,  
4 respectively. As a result, a fraction of the nanowires are observed to deposit onto the glass  
5 slide surface that is exposed to the AgNW suspension. Subsequently, 1 mL pure ethanol is  
6 flowed through the channel to remove excess nanowire suspension, followed by a gas  
7 purge and drying to remove liquid remaining inside the channel. AgNWs deposited on the  
8 top and bottom walls of the channel are not washed out with the main flow because the  
9 Van der Waal forces are of order  $10^{-6} \text{ N}$ <sup>36</sup> between the nanowire and the glass slide and are  
10 therefore strong enough to prevent the shear flow forces (of order  $10^{-9} \text{ N}$ ) from displacing  
11 the nanowire. At the end of the preparation process, a uniform thin layer of AgNWs forms  
12 at the surface of each glass slide as shown in Fig. 1B. The coated glass slides are then  
13 separated for further characterization.

14 As shown in Fig. 1C-E micrographs, nanowires coated on the surface of the glass slides  
15 exhibit increased alignment with increasing suspension flow rate through the channel. The  
16 deposited nanowires are poorly aligned at low flow rates, *i.e.* 0.5 mL/min, as shown in Fig.  
17 1C-i. With increasing flow rate, *i.e.* to 2 mL/min and 5 mL/min, the deposited nanowires  
18 begin to align along the flow direction over the whole area inside the microchannels (Fig.  
19 1C-ii and iii). While aspects of this flow alignment effect have been explored and utilized in  
20 previous studies,<sup>11,20,35,37,38</sup> the present experimental methods provide a simple and robust  
21 way to generate centimeter-scale and potentially patternable AgNW coatings on a flat  
22 substrate with high areal density and controlled alignment.

1

## 2 **Alignment of AgNWs**

3 We characterize the microscopic structure of nanowire networks by analyzing the  
4 micrographs obtained by both optical and scanning electron microscopy (SEM). Examples  
5 of micrographs are shown in Fig. 2A-C. They are taken from samples prepared at three  
6 different suspension flow rates: 0.5, 2, and 5 mL/min, respectively. For analysis, each  
7 individual nanowire in the field-of-view is approximated by a straight-line segment. The  
8 orientation,  $\vartheta$ , and length,  $l$ , of the AgNW are then recorded by image processing using  
9 software ImageJ. Here we define  $\theta = 0^\circ$  as the direction of the flow.

10 The distributions of the nanowire orientation are shown in the histograms of Fig. 2D.  
11 For the image in Fig. 2A, the probability distribution is very broad and flat, suggesting a  
12 predominately random distribution of the nanowire orientation. By contrast, the  
13 probability distribution of nanowire orientation from images in Fig. 2B and 2C exhibits a  
14 clear peak near  $\vartheta = 0^\circ$ . The presence of these peaks clearly demonstrates that the  
15 orientations of deposited AgNWs are biased toward the flow direction. These different  
16 distributions of nanowire orientation are also consistent with the intensity patterns  
17 generated by laser light scattering. As shown in the insets of Fig. 2E, the AgNW coating with  
18 random distribution of nanowire orientation exhibits a nearly isotropic scattering pattern  
19 in the  $k$ -space, while the one with aligned AgNWs exhibits a strongly anisotropic scattering  
20 pattern.

21 We further quantify alignment by the two-dimensional nematic order parameter defined  
22 as<sup>39,40</sup>



1 
$$S = 2 \langle \cos^2 \theta \rangle - 1 . \tag{1}$$

2 where  $S = 0$  corresponds to a random distribution, and  $S = 1$  corresponds to perfect  
3 alignment. Using the distribution of  $\theta$  in Fig. 2D, the three samples shown in Fig. 2A-C give  
4  $S$  values of 0.16, 0.61, and 0.84, respectively.

5 The shear rate near the glass surfaces plays an important role in controlling the degree  
6 of alignment of AgNWs in these flow-deposited coatings. Given the density,  $\rho$ , viscosity,  $\mu$ ,  
7 and flow rate,  $u$ , of the AgNW suspension, together with the geometry of the channel  
8 (height,  $H$ , and width,  $W$ ), the Reynolds' number,  $Re = \rho u H / \eta$ , is of order  $10^{-2}$ . This  
9 indicates that flow is laminar. Therefore, assuming no-slip boundary conditions, for a  
10 volumetric flow rate,  $Q$ , the shear rate near the wall can be calculated as  $\gamma = 6Q / (H^2 W)$ .  
11 In Fig. 2E, we plot the nematic alignment order parameter of the deposited AgNW coatings  
12 deposited versus shear rates. The suspended nanowires that have made point-contact with  
13 the glass surface respond to the high shear rate near the surface, introduced by the rapid  
14 channel flow, by adopting a preferred orientation parallel to the flow.

15 To better understand the flow-induced alignment behaviors, we perform semi-quantitative  
16 analyses on experimental observations. We first rule out gravity or sedimentation effects, since  
17 AgNWs adhere equally to both top and bottom surfaces of the thin channel. Therefore, a  
18 possible explanation for the effect of flow-induced alignment could derive from a competition  
19 between directional shear flow and random rotational diffusion of the AgNWs. At a low shear  
20 rate, the rotational diffusion dominates and gives rise to a more isotropic organization of the  
21 AgNWs, but at large shear rates the flow defines the orientation. We then estimate the Peclet  
22 number ( $Pe$ ) for the AgNW suspension, defined by the ratio between the shear rate and the

1 rotational diffusion constant of the nanowire,  $D_r$ , as<sup>33,41</sup>  $Pe = \dot{\gamma}/D_r = \pi\dot{\gamma}\mu L^3/4k_B T$ , where  
2  $\mu \approx 1.2 \text{ mPa} \cdot \text{s}$  is the viscosity of the AgNW suspension and  $L \approx 30 \text{ }\mu\text{m}$  is the average length  
3 of AgNWs. For the range of experimental shear rates,  $\dot{\gamma} = 10 \text{ to } 1000 \text{ s}^{-1}$ ,  $Pe$  is of the order of  
4  $10^6 \text{ to } 10^8$ . The large  $Pe$  imply that shear flow should dominate over rotational diffusion in all  
5 the experimental flow conditions used for preparing AgNW coatings. We believe that the key to  
6 the alignment of nanowires on the glass surface occurs when the rods make contact with the  
7 surface (*i.e.* rather than in the bulk fluid). Just after making contact, and assuming this contact  
8 occurs at one end of the nanowire with the other end free, the nanowires can pivot and will  
9 respond to flow shear-stresses near the surface. Here, the most plausible mechanism is a  
10 competition between electrostatic forces that pull the nanowire to the glass substrate and the  
11 hydrodynamic drag force of the shear flow that rotates the AgNWs along a direction parallel to  
12 the flow when they get contact with the glass surface. Here, by assuming a line charge density  
13  $\delta$  for the nanowire and a surface charge density  $\sigma$  for the glass surface, we can estimate the  
14 ratio between electrostatic torque ( $M_{elec}$ ) and hydrodynamic torque ( $M_{hydro}$ ),

$$15 \quad \frac{M_{hydro}}{M_{elec}} \sim \frac{4}{3} \frac{\gamma \eta L \epsilon_0 \epsilon_r}{\delta \sigma} \quad (2)$$

16 where  $\epsilon_0 \epsilon_r$  is the electrical permittivity of the AgNW suspension. The detailed illustration of  
17 those two torques can be found in the ESI. With the increasing shear rate,  $\gamma$ , it is possible to  
18 transition from an electrostatic-dominated regime to a shear-flow-dominated regime. In the  
19 former regime, AgNWs are pulled down to the glass surface with random orientations before  
20 they can be aligned by flow; in the latter region, AgNWs are quickly aligned by the high shear  
21 rate near the surface. In our experiments, given the glass surface charge on the order of  
22  $1 \text{ mC}/\text{m}^2$ , and a transition of shear rate at approximately  $\gamma = 100 \text{ s}^{-1}$ , according to Eq. 2, the

1 nanowires carry a line charge density on the order of  $3 \times 10^{-12} C/m$ , or 20 effective charges  
2 per micron. Although further experimental confirmation of these predictions is difficult, the  
3 estimation is plausible for the observed transition of the AgNW orientation as a function of the  
4 shear rate near the surface.

5

## 6 **Electrical conductivity and anisotropy**

7 One advantage of our system versus literature<sup>11</sup> is that we can break apart the  
8 microchannel to characterize the electrical resistance of the AgNW coatings on the surface  
9 of glass slides. To explore the angle-dependence of surface conductivity in our AgNWs  
10 coatings, we use a four-point probe setup and a rotating stage to measure the sheet  
11 resistance,  $R_s$ , at various angles,  $\theta$ , relative to the flow direction at the same location. The  
12 sheet resistances,  $R_s$ , of three AgNW coatings with different degrees of alignment are  
13 plotted in Fig. 3A as a function of  $\theta$ . For samples with good alignment, we find significant  
14 differences in measured sheet resistance at different angles. At the angle parallel to the flow  
15 direction, *i.e.*  $\theta = 0^\circ$  and  $180^\circ$ , the measured  $R_s$  are in the range of 3-5  $\Omega/sq$ . However, at  $\vartheta$   
16  $= 90^\circ$  and  $270^\circ$ ,  $R_s$  increases to  $\sim 42 \Omega/sq$ , *i.e.*, an order of magnitude higher. Accordingly,  
17 we extract the angle-dependent sheet resistance of these aligned samples as:

$$18 \quad R_{s,\theta} = a \sin(\theta) + R_0 . \quad (3)$$

19 Here  $a$  and  $R_0$  are fitting parameters. We find a good agreement between the data and the  
20 sinusoidal waveform. By contrast, the sheet resistance for an AgNW coating with random  
21 orientations show no angle dependence,  $\sim 3 \Omega/sq$ .

1           To further quantify the effect of alignment, we define the electrical anisotropy,  $\sigma_{ani}$ ,  
2 as the ratio between maximum and minimum sheet resistance measured at different angles,  
3 *i.e.*  $\sigma_{ani} = R_{s,max}/R_{s,min}$ , and we plot the ratio as a function of the AgNW coating order  
4 parameter,  $S$  (Fig. 3B). A strong anisotropy,  $\sigma_{ani}$  up to  $\sim 10$  is reached for highly aligned  
5 AgNW coatings ( $S = 0.84$ ). We note that alignment-induced electrical anisotropy has also  
6 been reported in coatings of carbon nanotubes (CNTs).<sup>40</sup> Our observations about the change  
7 of anisotropy with degree of alignment,  $S$ , are roughly consistent with the results measured  
8 for the CNT coatings, which is well-described by a model assuming a Gaussian distribution of  
9 the orientations of 1D conducting elements on a planar substrate. Anisotropy of electrical  
10 conductivity in aligned AgNW coatings has been reported. Ackermann *et al.*,<sup>42</sup> reported  $\sigma_{ani}$   
11 varying from 1.06 to 27.6. However, high electrical anisotropy, *i.e.*  $\sigma_{ani} > 2$ , was observed  
12 only in samples with sheet resistance larger than 100  $\Omega/\text{sq}$ . To our knowledge, the well-  
13 aligned AgNWs used in the present work are the first to exhibit a large anisotropy ( $\sim 10$ ) while  
14 maintaining low sheet resistance ( $< 50 \Omega/\text{sq}$ ) in all directions.

15

## 16 **Optical anisotropy**

17           Interestingly, the anisotropy of the coatings has a direct impact on their optical  
18 properties. We characterize the optical response of coatings made of aligned AgNW using  
19 the setup shown in Fig. 4A. In this setup, the sample is illuminated with a Tungsten halogen  
20 light source (HL-2000, Ocean Optics) at normal incidence angle (along  $-z$  direction), and the  
21 AgNW coatings are placed in the  $xy$ -plane. The camera or detector is placed in the  $xz$ -plane  
22 with the polar angle,  $\phi$ , measured relative to the  $z$ -axis. The angle between the polarization

1 of the incident light and the  $y$ -axis is defined as  $\alpha$ . For aligned AgNW coatings, the angle  
2 between the nanowire alignment direction and the  $y$ -axis is defined as  $\beta$ .

3 The images in Fig. 4B show the optical images of a well-aligned AgNW coating ( $S=0.84$ )  
4 with light polarized along the  $y$ -axis ( $\alpha = 0^\circ$ ) and  $x$ -axis ( $\alpha = 90^\circ$ ), recorded at  $\phi = 60^\circ$ . The  
5 sample appearance varies from orange to yellow-green when  $\alpha$  changes from  $0^\circ$  to  $90^\circ$ . In  
6 addition, a sharp decrease of the scattered light intensity occurs when  $\beta$  is rotated from  
7  $0^\circ$  to  $90^\circ$ , for both  $\alpha = 0^\circ$  and  $\alpha = 90^\circ$ . By contrast, the color and intensity from the  
8 coatings of poorly aligned AgNWs remain the same (Fig.5A, B)

9 We further investigate the color-changing mechanism by taking micrographs of the  
10 AgNW coatings using a microscope with a polarized light source. As shown in insets in Fig.  
11 4C, under the reflection mode, *i.e.*  $\phi = 0^\circ$ , and when the polarization and the AgNWs are  
12 aligned ( $\alpha = 0^\circ$  and  $\beta = 0^\circ$ ), the sample is mostly yellow. By contrast, the sample appears  
13 blue-green when the polarizer is perpendicular to the AgNW alignment ( $\alpha = 90^\circ$  and  $\beta =$   
14  $0^\circ$ ). In the transmission mode ( $\phi = 180^\circ$ ), the trends are opposite, as shown in insets in Fig.  
15 4D.

16 To more quantitatively explain the color differences, the reflectance and transmittance  
17 spectra are recorded. As shown in Fig. 4C, when  $\alpha = 0^\circ$ , the intensity of reflected light  
18 increases as a function of wavelength between 420 nm and 800 nm. When  $\alpha = 90^\circ$ ,  
19 however, the reflected intensity decreases. These findings are consistent with the colors  
20 observed from the optical microscope (insets in Fig. 4C).

21 The transmittance spectra recorded by the UV-Vis spectrometer are plotted in Fig. 4D.  
22 While we did not optimize for transparency, the films retained good light transmission

1 across the visible spectral range (~70%). The aligned AgNW coating exhibit absorbing  
2 valleys for illumination in both polarization directions. However, these two valleys are  
3 centered about two very different wavelengths. For  $\alpha = 0^\circ$  and  $\beta = 0^\circ$ , a strong  
4 absorption peak arises at long wavelengths, within the range of 600-650 nm, as shown in  
5 Fig 4D. For  $\alpha = 90^\circ$  and  $\beta = 0^\circ$ , the peak absorption arises at much shorter wavelengths,  
6 *i.e.*, ~380 nm. These spectra exhibit features similar to those of spectra reported for AgNWs  
7 in solution<sup>43</sup> and aligned AgNW bundles.<sup>30,33</sup> Prior simulation<sup>44</sup> and experimental<sup>11,33,45</sup>  
8 work explains the absorption peak at short (long) wavelength as due to the transverse  
9 (longitudinal) surface plasmon resonance (SPR) of the electrons in the AgNWs<sup>30</sup>. Specifically,  
10 the absorption peak at short wavelength is due to the transverse surface plasmonic  
11 resonances (SPRs) induced by electron oscillation along the AgNW diameter, and the  
12 absorption at the long wavelength is due to the longitudinal SPRs (induced parallel to the  
13 AgNW long axis). The broadening of the peaks could be due, in part, to the polydispersity  
14 in the AgNW distribution and to the coupling of electromagnetic waves among neighboring  
15 nanowires.

16 When stimulated by polarized light, the wavelength of the absorption peak depends  
17 on the angle between the individual nanowire and the light polarization. This angle-  
18 dependent absorption is clearly seen in micrographs of randomly oriented AgNWs in **Fig.**  
19 **5E** and **5F**, where an individual AgNW imaged in transmission appears yellow or green  
20 depending on its orientation relative to the light polarization. However, because of the  
21 random orientation of AgNWs, the overall spectra of the whole AgNW coating does not  
22 show absorption valleys, as seen in Fig. 5C and 5D. By contrast, when AgNWs are aligned

1 along the same direction, the SPR absorption spectra of the aligned individual AgNWs are  
2 approximately the same and the sample as a whole exhibits a clear valley in its transmission  
3 spectra, as shown in Fig 4D and 4E.

4 We systematically quantify the angle-dependent light intensity under various  
5 illumination and observation configurations to fully explore the optical anisotropy of the  
6 strongly aligned AgNW coating ( $S=0.84$ ) at 650 nm. The polar plot in Fig. 6A shows the  
7 intensity,  $I$ , of the reflected light, *i.e.*  $\phi = 0^\circ$ , as a function of the angle between the  
8 input polarizer and the AgNW alignment direction. The plot in Fig. 6A clearly  
9 demonstrates optical anisotropy; however, the value,  $\frac{I_{max}}{I_{min}} = 1.7$ , is rather small and  
10 the normalized light intensity peak at  $180^\circ$  is quite broad with Full-Width-at-Half-  
11 Maximum (FWHM) of approximately  $92^\circ$ . This result is consistent with previous studies  
12 where weak optical anisotropy ( $<2\times$ ) is observed from individual aligned nanotubes and  
13 from AgNWs in both transmission and reflection modes.<sup>10,11,46</sup>

14 Next, we illuminate the aligned AgNW coating with unpolarized light and measure  
15 the intensity of scattered light at  $\phi = 60^\circ$ ; for this measurement, the angle of aligned  
16 AgNW coating,  $\beta$ , is varied by rotating the sample. The results are shown in Fig. 6B, which  
17 exhibits a large anisotropy,  $\frac{I_{max}}{I_{min}} = 7.2$ , and a narrow peak of normalized intensity with  
18 FWHM of approximately  $24^\circ$ . For comparison, the intensity of unpolarized light  
19 scattered by a coating with randomly oriented AgNWs shows no variation as a function  
20 of  $\beta$ . These results indicate that the coating with aligned AgNWs scatters more light in  
21 the direction perpendicular to the AgNW alignment direction, and less light in the

1 direction parallel to the alignment direction. This type of effect is observed in optical  
2 gratings with parallel stripe structure on the surface.<sup>47</sup> It is also worth noting that the  
3 aligned AgNW coating scatters less light in total when integrating over  $\beta$ , compared to  
4 a randomly oriented AgNW coating. This scattering could potentially affect  
5 the haze of the coating. Reduction of haze by alignment has been studied previously<sup>31</sup>  
6 and is expected to decrease with better alignment, but we leave quantification of haze  
7 in our samples for future work.

8 Finally, we combine the two anisotropic effects by measuring the intensity of light  
9 scattered from polarized light source. Specifically, for  $\alpha = 0^\circ$ , and the intensity of  
10 scattered light at a constant azimuthal  $\phi = 60^\circ$  is measured as a function of different  
11 angles  $\beta$ . As shown in Fig. 6C, this configuration produces a very large optical anisotropy,  
12 with  $\frac{I_{max}}{I_{min}} = 25.6$ , and a very narrow peak, with FWHM of approximately  $15^\circ$ . The  
13 comparison of normalized light intensity versus  $\beta$  for various values of  $\alpha$  is shown in Fig.  
14 6D. Clearly, the directional alignment of AgNWs and the polarization optical absorption  
15 and scattering properties of the individual AgNWs contribute to overall optical anisotropy  
16 of the well-aligned AgNW coating. When the two mechanisms are combined, we observe  
17 a much higher anisotropy than reported in earlier studies.<sup>10,11,46</sup>

18 Large optical anisotropy has been shown to improve the resolution of signals such as  
19 those arise in polarization images or surface-enhanced Raman spectroscopy (SERS),<sup>30</sup> and  
20 large anisotropy is desirable in nanowire-based polarizers for polarization light sensors.  
21 Normally, researchers can use the different responses of aligned metal nanowires under  
22 different polarization light conditions to achieve the optical anisotropy. Previous studies



1 showed that transmission or reflection modes typically give an optical anisotropy of less  
2 than  $2x$ ,<sup>11,25</sup> in agreement with the results shown in Fig. 6A. Here, we have uncovered a  
3 novel way to further increase the optical anisotropy that relies on the light *scattered* by the  
4 aligned AgNWs. This detection configuration, wherein well-aligned AgNW coatings are  
5 illuminated with polarized light and the light scattered by the coating is detected at  
6 different polar angles, takes advantage of both the intrinsic polarization properties of  
7 AgNWs and the angle-dependent scattering of aligned the AgNWs to achieve greater optical  
8 anisotropy, which can be as large as 25x as demonstrated in Fig. 6C.

9

## 10 **Conclusions**

11 We developed a simple and robust flow-induced alignment method for preparing  
12 centimeter-scale planar conductive silver nanowire coatings with high degrees of anisotropy.  
13 Specifically, we demonstrated patterning of a 5 mm by 2 cm film strip of AgNWs with an  
14 orientational order parameter that was tunable from 0.16 to 0.84 and had concomitant  
15 variation in electrical and optical anisotropy. The alignment can be tuned by varying the shear  
16 rate of nanowire suspension near the substrate during the deposition process. As a result of the  
17 preferred direction of AgNWs, coatings consisting of highly aligned AgNWs exhibit large  
18 anisotropy in both electrical conductivity and optical properties. For electrical conductivity, an  
19 anisotropy of  $\sim 10x$  is achieved, while the overall sheet resistance remains low. A very large  
20 optical anisotropy of  $\sim 25x$  is observed in the scattered polarized light due to the combination of  
21 the intrinsic polarization property of individual AgNWs and “grating” effects of the aligned  
22 AgNWs network. Those highly conductive transparent coatings with large electrical and

1 optical anisotropy can be potentially used for design of novel flexible antennas, polarized-  
2 light-based sensors, and for surface enhanced Raman spectroscopy.

3

#### 4 **Experimental section**

5 **Silver Nanowire Suspension.** The silver nanowires (AgNWs) were purchased from  
6 BlueNano (SLV-NW-90). The average length and diameter of the nanowires are  $30\pm 5\ \mu\text{m}$   
7 and  $90\pm 20\ \text{nm}$ , respectively. The nanowires are suspended in ethanol at a solid  
8 concentration of  $\sim 1\ \text{wt}\%$ . The nanowire suspension was used as-received.

9

10 **Assembly of The Microfluidic Channel.** To fabricate the channels, two glass slides are  
11 attached (sandwiched) using two strips of double-sided tape, leaving a thin gap, as shown  
12 in **Fig. 1A**. The resulting rectangular channels are typically 25 mm in length, 5 mm in width,  
13 and 200 to 600  $\mu\text{m}$  in height. The two open ends of the channel are then connected to a  
14 syringe filled with AgNW suspension and a waste bottle.

15

16 **Electrical Characterization.** The sheet resistances of the resulting AgNW coatings are  
17 measured using a four-point probe setup to eliminate the effect of contact resistance  
18 between the electrodes and coatings. Four electrical probes made of thin gold wires are  
19 arranged to be parallel and equally spaced. The part of the probe that contacts the  
20 nanowire coating has length  $w = 2\ \text{mm}$ , and each probe is separated by  $d = 0.5\ \text{mm}$ , as  
21 shown in Fig. S3 in ESI. A constant DC current,  $I$ , is applied through the two outmost probes,  
22 and the voltage,  $U$ , is measured between the two inner probes. The sheet resistance,  $R_s$ , is

1 then calculated by

$$2 \quad R_s = \frac{U w}{I d}, \quad (3)$$

3 where  $R_s$  has a unit of  $\Omega/\text{sq}$ . This setup permits measurement of the intrinsic electrical  
4 conductivity of the nanowire coatings. To explore the angle-dependence of surface  
5 conductivity of our AgNWs coatings, we place the coatings on a rotating stage wherein  $R_s$   
6 can be measured at various angles relative to the flow direction at the same location.

7

8 **Optical characterization.** The micrographs of AgNW samples are recorded using an optical  
9 microscope (Olympus BX61) in both transmission and reflectance modes. In addition, the  
10 reflectance and transmittance spectra are recorded by coupling, respectively, a fiber  
11 spectrometer (USB4000, Ocean Optics) and a UV-Vis spectrometer (Cary 5000, Agilent  
12 Technologies) to the Olympus microscope.

13

## 14 **Acknowledgements**

15 We thank Prof. Karen Winey for helpful discussions. The project is supported by the National  
16 Science Foundation through DMR16-07378, MRSEC DMR-1720530, including both its Optical  
17 Microscopy and its Properties Measurement Shared Experimental Facilities, MRSEC DMR11-  
18 20901, and NASA NNX08AO0G. This work is also supported in part by Fundamental Research  
19 Funds for the Central Universities, the National Natural Science Foundation of China through  
20 Grants No. 11674019 (Y.X.) and 11604045 (D.G.), Projects from Shanghai Science & Technology  
21 Commission 17JC1400700 and 17ZR1440000, and Shanghai Pujiang Program 16PJ1400100 (D.  
22 G.).

1

## 2 **Author Contributions**

3 Y.X., D.G., and A.G.Y. conceived and designed the project; Y.X., G.A.C., A.A., and D.K. carried out  
4 experiments for sample preparation; Y.X., A.L.E., and J.M.K. carried out electric characterization  
5 experiments; D.G. and C.B. carried out optical characterization experiments; Y.X., D.G., R.D., and  
6 A.G.Y. analyzed the data and wrote the manuscript. All authors discussed the results and  
7 commented on the manuscript.

8

9

## References

10

- 11 1. D. J. Finn, M. Lotya and J. N. Coleman, *ACS Applied Materials & Interfaces*, 2015, **7**, 9254-  
12 9261.
- 13 2. J. Liang, K. Tong and Q. Pei, *Advanced Materials*, 2016, **28**, 5986-5996.
- 14 3. E. M. Freer, O. Grachev, X. Duan, S. Martin and D. P. Stumbo, *Nat. Nanotechnol.*, 2010, **5**,  
15 525-530.
- 16 4. F. Xu and Y. Zhu, *Adv. Mater.*, 2012, **24**, 5117–5122-5117–5122.
- 17 5. L. Hu, H. S. Kim, J. Y. Lee, P. Peumans and Y. Cui, *ACS Nano*, 2010, DOI: 10.1021/nn1005232.
- 18 6. J. Yao, H. Yan, S. Das, J. F. Klemic, J. C. Ellenbogen and C. M. Lieber, *Proceedings of the*  
19 *National Academy of Sciences*, 2014, DOI: 10.1073/pnas.1323818111.
- 20 7. D. Rossouw, M. Couillard, J. Vickery, E. Kumacheva and G. A. Botton, *Nano Letters*, 2011,  
21 **11**, 1499-1504.
- 22 8. L. Song, A. C. Myers, J. J. Adams and Y. Zhu, *ACS Applied Materials & Interfaces*, 2014, **6**,  
23 4248-4253.
- 24 9. L. Lu, L.-L. Wang, C.-L. Zou, X.-F. Ren, C.-H. Dong, F.-W. Sun, S.-H. Yu and G.-C. Guo, *The*  
25 *Journal of Physical Chemistry C*, 2012, **116**, 23779-23784.
- 26 10. X. Ma, X. Zhu, F. You, J. Feng, M.-C. Wang and X. Zhao, *Journal of Alloys and Compounds*,

- 1 2014, **592**, 57-62.
- 2 11. J. W. Liu, J. L. Wang, W. R. Huang, L. Yu, X. F. Ren, W. C. Wen and S. H. Yu, *Sci Rep*, 2012,  
3 **2**, 987.
- 4 12. R. Mutiso and K. Winey, *Phys. Rev. E: Stat., Nonlinear, Soft Matter Phys.*, 2013, **88**.
- 5 13. R. M. Mutiso, M. C. Sherrott, A. R. Rathmell, B. J. Wiley and K. I. Winey, *ACS nano*, 2013.
- 6 14. S. White, B. DiDonna, M. Mu, Lubensky and K. Winey, *Phys. Rev. B*, 2009, **79**.
- 7 15. D. Zhang, Y. Xiang, J. Chen, J. Cheng, L. Zhu, R. Wang, G. Zou, P. Wang, H. Ming, M.  
8 Rosenfeld, R. Badugu and J. R. Lakowicz, *Nano letters*, 2018, **18**, 1152-1158.
- 9 16. A. W. Sanders, D. A. Routenberg, B. J. Wiley, Y. Xia, E. R. Dufresne and M. A. Reed, *Nano*  
10 *Letters*, 2006, **6**, 1822-1826.
- 11 17. W. Wang, Q. Yang, F. Fan, H. Xu and Z. L. Wang, *Nano letters*, 2011, **11**, 1603-1608.
- 12 18. X. Guo, M. Qiu, J. Bao, B. J. Wiley, Q. Yang, X. Zhang, Y. Ma, H. Yu and L. Tong, *Nano Letters*,  
13 2009, **9**, 4515-4519.
- 14 19. D. Lei, A. Aubry, Y. Luo, S. A. Maier and J. B. Pendry, *ACS Nano*, 2011, **5**, 597-607.
- 15 20. S.-k. Duan, Q.-l. Niu, J.-f. Wei, J.-b. He, Y.-a. Yin and Y. Zhang, *Phys. Chem. Chem. Phys.*,  
16 2015, **17**, 8106-8112.
- 17 21. Y. Jeon, H. Kang, S. Ko and H. Sung, *Measurement Science and Technology*, 2013, DOI:  
18 10.1088/0957-0233/24/3/035303.
- 19 22. Y. Li and Y. Wu, *Journal of the American Chemical Society*, 2009, DOI: 10.1021/ja9000882.
- 20 23. Y. Liu, J.-H. Chung, W. Liu and R. S. Ruoff, *The Journal of Physical Chemistry B*, 2006, DOI:  
21 10.1021/jp061367e.
- 22 24. S. J. Papadakis, Z. Gu and D. H. Gracias, *Appl. Phys. Lett.*, 2006.
- 23 25. H.-Y. Shi, B. Hu, X.-C. Yu, R.-L. Zhao, X.-F. Ren, S.-L. Liu, J.-W. Liu, M. Feng, A.-W. Xu and S.-  
24 H. Yu, *Advanced Functional Materials*, 2010, **20**, 958-964.
- 25 26. W. Yang, L. Qu, R. Zheng, Z. Liu, K. R. Ratinac, L. Shen, D. Yu, L. Yang, C. J. Barrow, S. P.  
26 Ringer, L. Dai and F. Braet, *Chemistry of Materials*, 2011, DOI: 10.1021/cm1033645.
- 27 27. R. Zhu, Y. Lai, V. Nguyen and R. Yang, *Nanoscale*, 2014, DOI: 10.1039/C4NR02645D.
- 28 28. L. Meng, R. Bian, C. Guo, B. Xu, H. Liu and L. Jiang, *Advanced Materials*, 2018, **30**, 1706938.
- 29 29. C. D. Preston, L. Hu and L. J. Martínez-Miranda, *Molecular Crystals and Liquid Crystals*,

- 1           2015, **610**, 235-239.
- 2   30.   A. Tao, F. Kim, C. Hess, J. Goldberger, R. He, Y. Sun, Y. Xia and P. Yang, *Nano Lett.*, 2003,  
3           **3**, 1229-1233.
- 4   31.   S. Kang, T. Kim, S. Cho, Y. Lee, A. Choe, B. Walker, S. J. Ko, J. Y. Kim and H. Ko, *Nano Lett.*,  
5           2015, **15**, 7933-7942.
- 6   32.   Y. Ko, S. K. Song, N. H. Kim and S. T. Chang, *Langmuir*, 2016, **32**, 366-373.
- 7   33.   B. Park, I. G. Bae and Y. H. Huh, *Sci Rep*, 2016, **6**, 19485.
- 8   34.   S. Cho, S. Kang, A. Pandya, R. Shanker, Z. Khan, Y. Lee, J. Park, S. L. Craig and H. Ko, *ACS*  
9           *Nano*, 2017, **11**, 4346-4357.
- 10 35.   Y. Huang, X. Duan, Q. Wei and C. M. Lieber, *Science*, 2001, **291**, 630-633.
- 11 36.   F. L. Leite, C. C. Bueno, A. L. Da Roz, E. C. Ziemath and O. N. Oliveira, *Int J Mol Sci*, 2012,  
12           **13**, 12773-12856.
- 13 37.   S. B. Kharchenko, J. F. Douglas, J. Obrzut, E. A. Grulke and K. B. Migler, *Nature Materials*,  
14           2004, DOI: 10.1038/nmat1183.
- 15 38.   M. Liu, Y. Chen, Q. Guo, R. Li, X. Sun and J. Yang, *Nanotechnology*, 2011.
- 16 39.   P. J. Steinhardt, D. R. Nelson and M. Ronchetti, *Physical Review B*, 1983, **28**, 784-805.
- 17 40.   C. Zamora-Ledezma, C. Blanc, N. Puech, M. Maugey, C. Zakri, E. Anglaret and P. Poulin,  
18           *Physical Review E*, 2011, **84**, 62701.
- 19 41.   M. Doi and S. F. Edwards, *The theory of polymer dynamics*, oxford university press, 1988.
- 20 42.   T. Ackermann, R. Neuhaus and S. Roth, *Sci Rep*, 2016, **6**, 34289.
- 21 43.   Q. N. Luu, J. M. Doorn, M. T. Berry, C. Jiang, C. Lin and S. P. May, *Journal of colloid and*  
22           *interface science*, 2011, **356**, 151-158.
- 23 44.   J. Dong and I. A. Goldthorpe, *Nanotechnology*, 2017, **29**, 45705.
- 24 45.   B. Pietrobon, M. McEachran and V. Kitaev, *ACS Nano*, 2009, **3**, 21-26.
- 25 46.   M. F. Islam, D. E. Milkie, C. L. Kane, A. G. Yodh and J. M. Kikkawa, *Physical Review Letters*,  
26           2004, **93**, 37404.
- 27 47.   G. J. Dunning and M. L. Minden, *Applied Optics*, 1980, **19**, 2419.
- 28
- 29

1 Table 1: Comparison of electrical and optical properties of AgNW films prepared with  
 2 different aligning methods

Sample preparation	Alignment quantified ?	Areal density/fraction	Sheet resistance	Electrical anisotropy	Transparency	Linear Optical Anisotropy	Patterning?	Scale
Self-assembly at water-oil interface <sup>25</sup>	N	Close-packed	NM	NM	NQ	NQ	N	10 mm
Langmuir-Blodgett <sup>30</sup>	N	Close-packed	NM	NM	NQ[a]	NQ	N	50 mm
Flow through circular capillary tube <sup>11</sup>	N	NQ[b]	NM	NM	NQ	~2	N	300 $\mu$ m[c]
Capillary printing <sup>31</sup>	Y	0.3-20%	10-50 $\Omega$ /sq	~1.7	90-95%	NM	N	~10mm
Meniscus-dragging <sup>32</sup>	N	3-12x10 <sup>4</sup> NW/m <sup>2</sup>	10 $\Omega$ /sq	NM	70-95%	1.5	N	~10mm
Dip-coating <sup>42</sup>	Y	0.3-2.6%	50-10 <sup>7</sup> $\Omega$ /sq	1.06-27.6	97-99%	NM	N	~25mm
H-dip <sup>33</sup>	N	NQ	2-7 $\Omega$ /sq	1.2	60-80%	2-3	N	~100mm
bar-coating <sup>34</sup>	Y	NQ[b]	NA	NA	80-95%	~4	N	200mm
Microfluidics (this work)	Y	10 <sup>4</sup> NW/mm <sup>2</sup>	3-5 $\Omega$ /sq	~10	70-80%	~25	Y	~5mm wide

3 Note:

4 Y: Yes; N: No; NM: Not measured; NQ: Not quantified

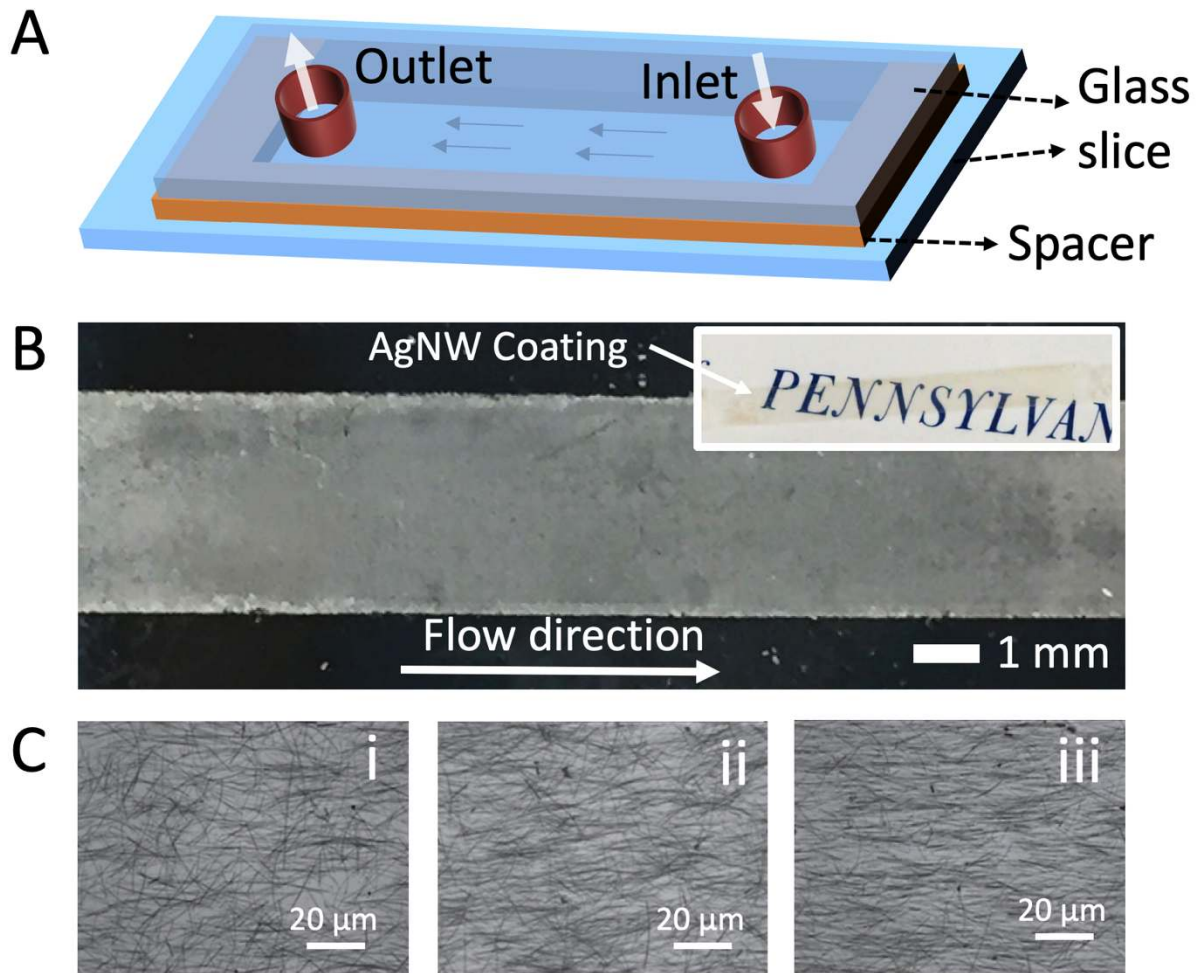
5 [a] Transmission spectra were measured but the intensities were not quantified

6 [b] Micrographs of nanowire coatings were shown but the areal densities were not quantified.

7 [c] Diameter of the inner surface of the capillary tube

8

1

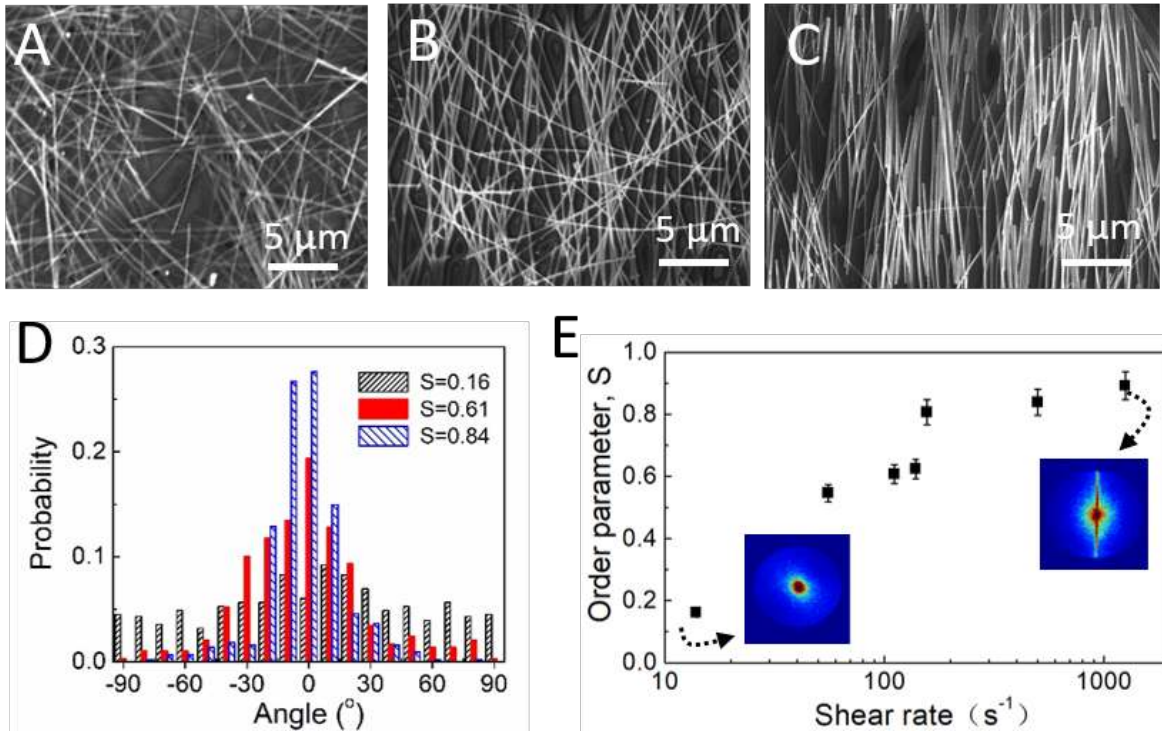


2 Fig. 1: (A) Schematic of flow channels for preparing silver nanowire coatings. (B) Low  
3 magnification optical image of the deposited AgNW coating of approximately 40% areal  
4 coverage, showing centimeter-scale uniformity. Inset: Photograph of the same AgNW  
5 coating taken on top of the text, showing its transparency. (C) High magnification optical  
6 images of AgNW deposited under different flow conditions. The shear rates of AgNW  
7 suspension near the glass substrate are  $15 \text{ s}^{-1}$ (i),  $100 \text{ s}^{-1}$ (ii), and  $500 \text{ s}^{-1}$  (iii), respectively.

8



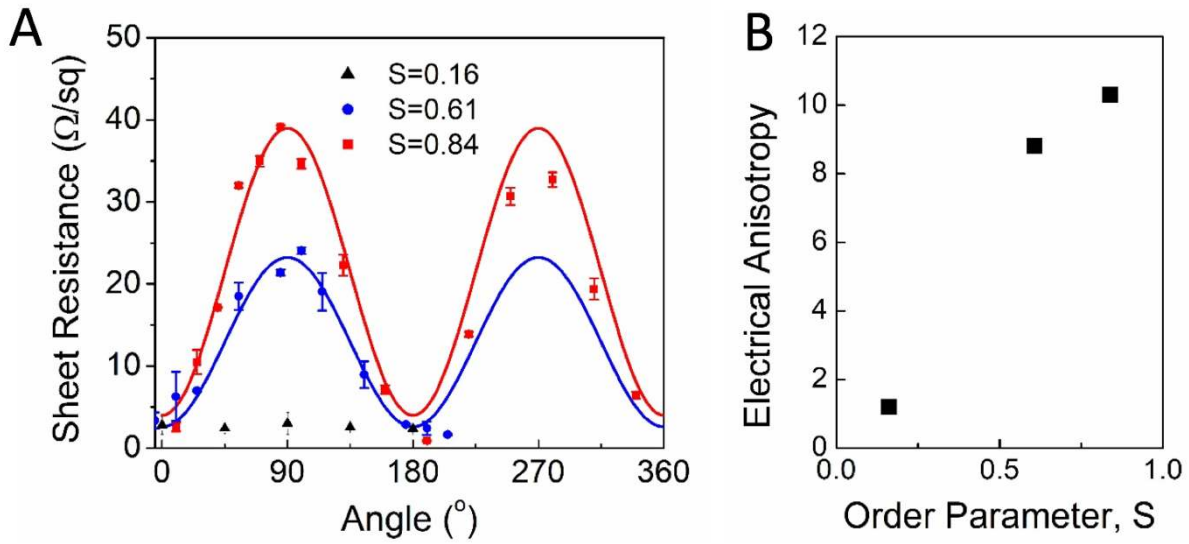
1



2 Fig. 2: (A-C) SEM images of three AgNW coatings to illustrate analysis of the orientations of  
3 individual nanowires. (D) Histogram of the angle between the nanowire orientation and  
4 flow direction for three representative samples seen in Fig. 1C with different order  
5 parameters:  $S=0.16$  (A),  $S=0.61$  (B), and  $S=0.84$  (C). (E) Order parameter of deposited AgNW  
6 coatings,  $S$ , as a function of shear rate of the flowing AgNW suspensions near the glass  
7 substrate,  $\gamma$ . Insets: Light scattering patterns of a random and well-aligned AgNW coating  
8 in  $k$ -space. The colors show the intensity of the scattered laser light with red as the highest  
9 intensity and blue as the lowest intensity.

10

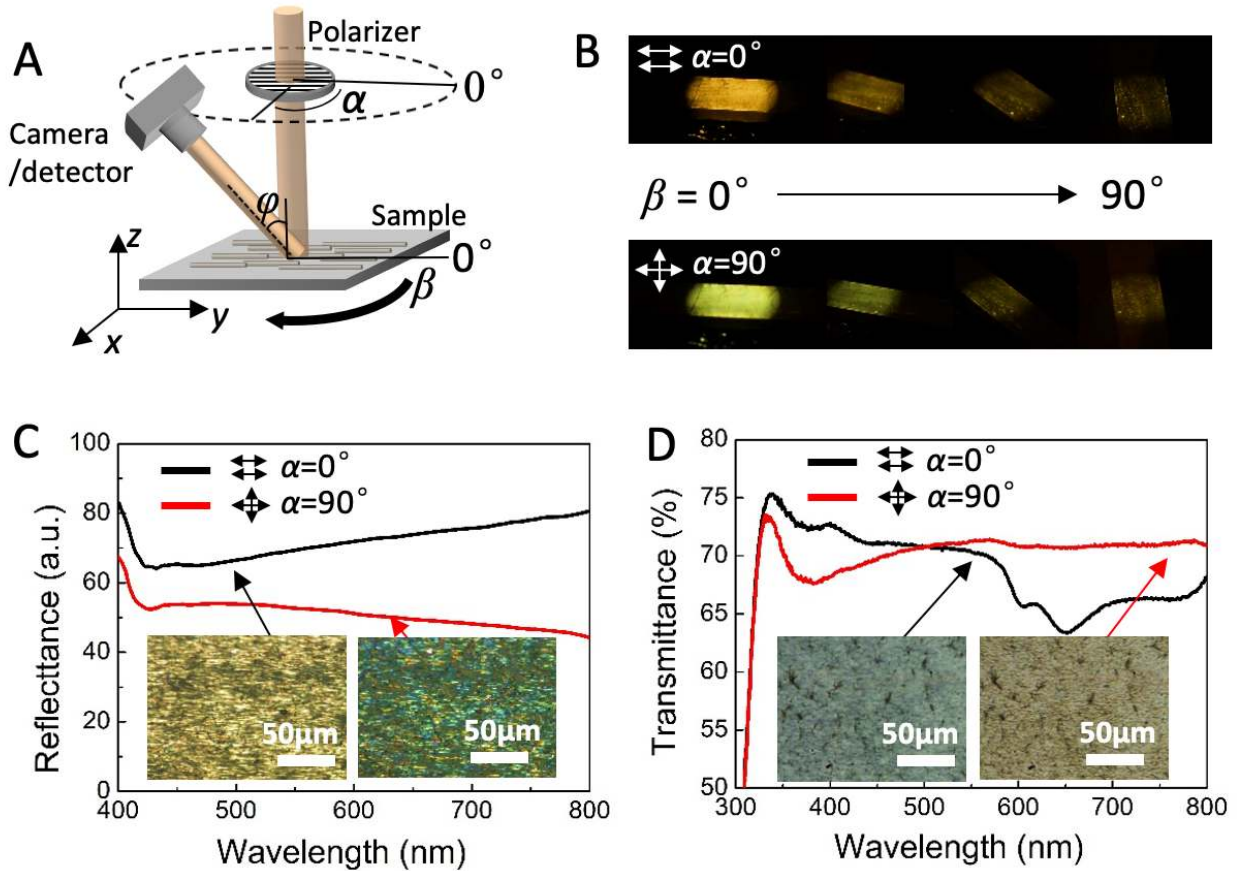
1



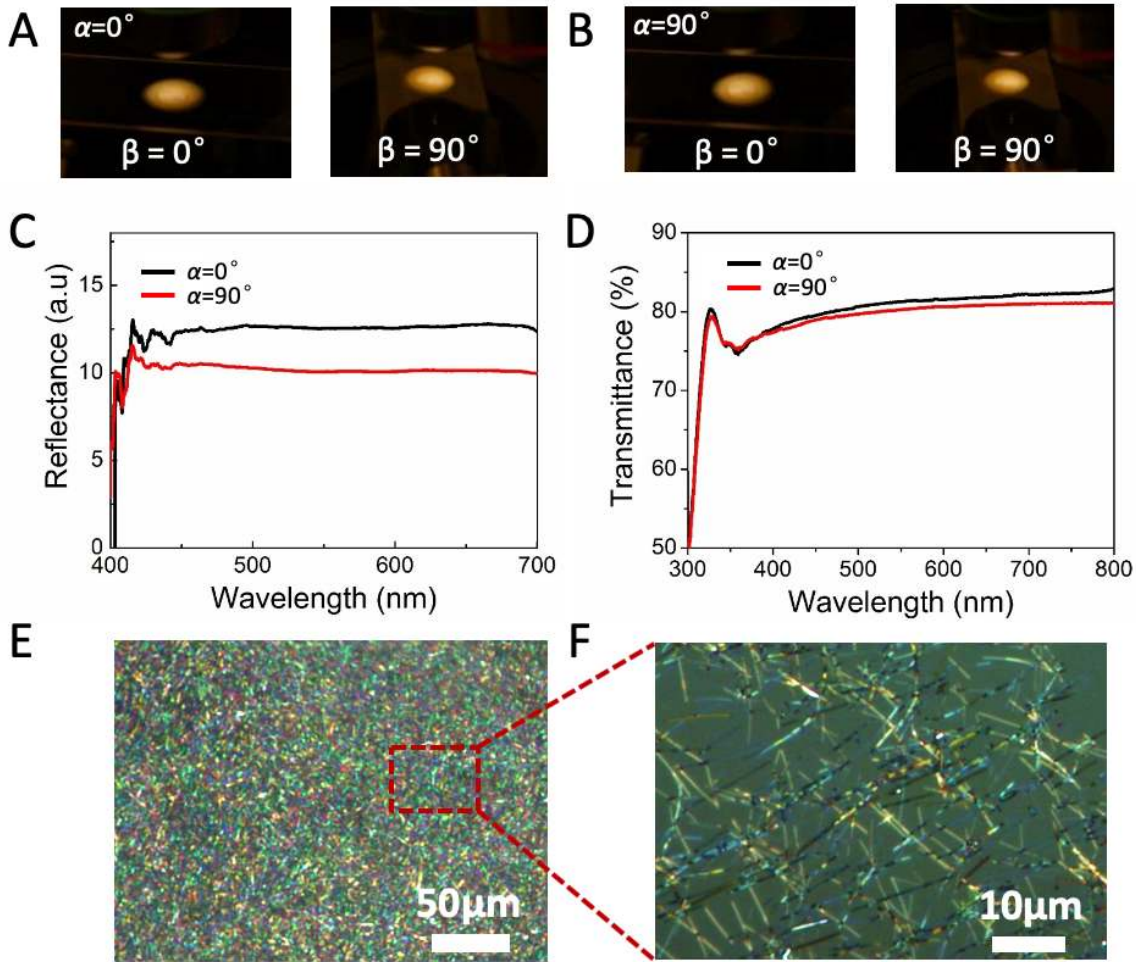
2

3 Fig. 3: Angle-dependent sheet resistance of the AgNW coatings. (A) Sheet resistance as a  
4 function of measurement angle relative to the alignment of the AgNW coatings (*i.e.*, with  
5 order parameters of 0.84, 0.61, 0.16. Solid lines are fits to a sinusoidal function; (B) Electrical  
6 anisotropy as a function of order parameter.

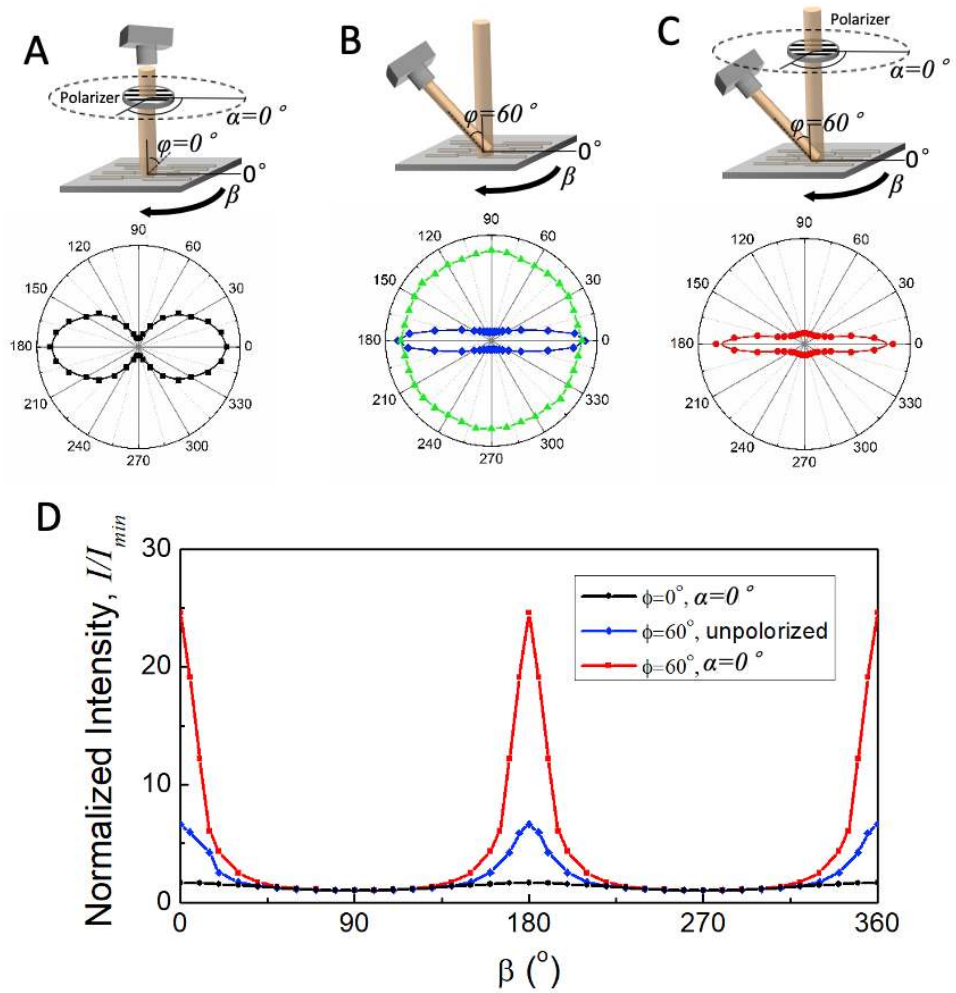
7



1  
 2 Fig. 4: Angle-dependent optical properties of the aligned AgNW coating ( $S=0.84$ ) under  
 3 polarized illumination. (A) Schematic of the optical measurement setup showing angles of  
 4 AgNW alignment ( $\beta$ ), polarization of incident light ( $\alpha$ ), and observation location ( $\phi$ ). (B)  
 5 Photos taken at  $\phi = 60^\circ$  and various  $\beta$  angles when the incident light is polarized parallel  
 6 (top) and perpendicular (bottom) to the AgNW alignment direction. (C) Spectrum of  
 7 reflected light for two different input polarization configurations: parallel (black line) and  
 8 perpendicular (red line) to the AgNW alignment direction. Inset: Optical micrographs of  
 9 AgNW coating in reflection. (D) Spectrum of transmitted light under parallel and  
 10 perpendicular illumination. Inset: Optical micrographs of AgNW coating in the transmission  
 11 mode.



1  
 2 Fig. 5: Angle-independent *optical appearance and spectrum of randomly oriented AgNW*  
 3 *coatings under polarized light.* (A) and (B) are photos of a random AgNW coating taken at  
 4 various  $\beta$  angles, under incident polarization of  $\alpha = 0^\circ$  (A) or  $\alpha = 90^\circ$  (B) Isotropic coatings  
 5 appear the same under different polarization and observation angles; (C) and (D) Spectra of  
 6 reflected and transmitted light by randomly oriented AgNW coatings. (E) Micrograph of a  
 7 randomly orientated AgNW coating under polarized light showing colors due to distributions  
 8 of individual nanowires; (F) Zoom-in view showing individual AgNWs that exhibit different  
 9 colors depending on their orientations.



1  
2  
3 Fig. 6: Angle-dependent light intensity from aligned AgNW coatings. (A) Reflected light  
4 intensity ( $\phi = 0^\circ$ ) as a function of  $\beta$  angles when the incident light (650nm) is polarized  
5 parallel to the AgNW alignment direction ( $\alpha = 0^\circ$ ); (B) Scattered light intensity ( $\phi = 60^\circ$ )  
6 as a function of  $\beta$  when a random (green) and well-aligned (blue,  $S=0.84$ ) AgNW coatings are  
7 illuminated with *unpolarized* light; (C) Scattered light intensity ( $\phi = 60^\circ$ ) as a function of  $\beta$   
8 when the incident light is polarized parallel to the AgNW alignment direction ( $\alpha = 0^\circ$ ); (D)  
9 Normalized light intensity vs.  $\beta$  for a well-aligned AgNW ( $S=0.84$ ) coating under different  
10 illuminating and observation configurations.